1   Classifying cold stress responses of inbred maize seedlings using RGB imaging

2

3   Tara A. Enders[1], Susan St. Dennis[1], Justin Oakland[1], Steven T. Callen[2,5], Malia A. Gehan[2],
4   Nathan D. Miller[3], Edgar P. Spalding[3], Nathan M. Springer[1], Cory D. Hirsch[4]

5

6   [1]Department of Plant and Microbial Biology, University of Minnesota, St. Paul, MN 55108
7   [2]Donald Danforth Plant Science Center, St. Louis, MO 63132
8   [3]Department of Botany, University of Wisconsin-Madison, Madison, Wisconsin 53706
9   [4] Department of Plant Pathology, University of Minnesota, St. Paul, MN 55108
10   [5]Current affiliation: Bayer U.S. Crop Science, St. Louis, MO 63167
11
12   Corresponding author: Cory D. Hirsch (cdhirsch@umn.edu)

13

14   4-6 keywords: Maize, cold stress, phenotyping, necrosis, seedling growth

15

Abstract

17   Increasing the tolerance of maize seedlings to low temperature episodes could mitigate the
18   effects of increasing climate variability on yield. To aid progress toward this goal, we established
19   a growth chamber-based system for subjecting seedlings of 40 maize inbred genotypes to a
20   defined, temporary cold stress while collecting digital profile images over a 9-day time course.
21   Image analysis performed with PlantCV software quantified shoot height, shoot area, 14 other
22   morphological traits, and necrosis identified by color analysis. Hierarchical clustering of changes
23   in growth rates of morphological traits and quantification of leaf necrosis over two time intervals
24   resulted in three clusters of genotypes, which are characterized by unique responses to cold
25   stress. For any given genotype, the set of traits with similar growth rates is unique. However, the
26   patterns among traits are different between genotypes. Cold sensitivity was not correlated with
27   the latitude where the inbred varieties were released suggesting potential further improvement
28   for this trait. This work will serve as the basis for future experiments investigating the genetic
29   basis of recovery to cold stress in maize seedlings.

Introduction

Climate change threatens to negatively impact performance of many important crops, including maize. Extreme heat and drought in maize can cause decreases in yield, especially during later stages of development (Sánchez et al., 2014). One method of avoiding yield losses due to extreme heat and drought late in the season is to plant crops earlier in the season (Kucharik, 2008); however, earlier planting increases the risk of exposing maize seedlings to low temperature stress conditions.

Cold stress is often described as a freezing stress (≤ 0°C) or a chilling stress (generally above 0°C and below 15°C) across plant species (Lyons, 1973; Greaves, 1996). Suboptimal temperatures can have multiple impacts on plant growth depending on the severity and developmental time point at which the stress occurs. Effects can range from slight delays in development from growth inhibition to plant death. Other commonly observed stress responses include leaf chlorosis and necrotic lesions (Yadav, 2010).

As a species, maize is considered cold-sensitive (Sellschop and Salmon, 1928); however, genetic variation in cold sensitivity exists among inbreds (Greaves, 1996). Several studies have considered maize genotypes that display mild cold sensitive phenotypes to be cold tolerant, despite the lines still being affected by cold stress (Janowiak and Dörffling, 1996; Fracheboud et al., 1999; Sowiński et al., 2005; Wijewardana et al., 2015). However, it is difficult to try to compare levels of sensitivity across studies done under different growth conditions, different temperatures, and at different developmental stages. Also, previous studies have rarely analyzed more than two maize genotypes at a time. Greaves (1996) stated that to improve plant performance under low temperature conditions, genetic variation needed to be characterized for multiple traits, such as levels of tissue injury and growth rates. To identify optimal genetic material for breeding programs interested in maximizing cold tolerance in maize, it is essential to thoroughly characterize the range of cold sensitivity.

Many physiological processes in plants are impeded by low temperatures, such as photosynthetic capacity, membrane rigidity, transpiration, and enzyme activity (Marocco et al., 2005). Together, these physiological effects of cold stress can result in poor agronomic performance, such as slower emergence, decreased biomass accumulation, reduced growth rates, and leaf chlorosis and necrosis (Miedema, 1982). Relative growth rates (Hetherington and Oquist, 1988; Verheul et al., 1996), electrolyte leakage assays (Capell and Dörffling, 1993), and photosynthesis related measurements (Hetherington and Oquist, 1988; Aguilera et al., 1999) have been used in several studies to classify maize seedling responses to cold stress. These approaches require destructive measurements of plants, and therefore necessitate more individuals and space to collect time course data. However, some measurements have been conducted in a non-destructive manner. In field conditions, necrotic injury was visually assessed on a relative scale at a single time point on six genotypes, where lines with the least amount of leaf necrosis were classified as cold tolerant (Janowiak et al., 2003). An alternative approach to destructive and manual assessment is to move to image-based plant phenotyping methods to allow for robust measures of changes in color and growth without destructive, subjective, or labor-intensive techniques.

There are a growing number of commercial and custom-built systems for integrated controlled plant growth and imaging (Tisné et al., 2013). Currently available commercial systems can provide valuable insight into variation in plant growth and development, but they tend to have higher costs and infrastructure requirements that limit access to a small number of researchers. Additionally, these systems usually restrict researchers to conducting a single experiment at a time. We sought to develop an image-based approach that could be implemented easily to document morphological traits of maize seedlings at a low cost. This system is not fully

78 automated because it requires manual plant staging. As manual staging of plants is required,
79 we have implemented tools to ensure high-quality standardized images are captured.

80 Many researchers have, or are currently developing, custom low-cost phenotyping platforms to
81 fit their needs. Our system is not necessarily unique in this pursuit and is similar to other
82 recently developed low-cost imaging systems (Knecht et al., 2016; Armonienė et al., 2018;
83 Czedik-Eysenberg et al., 2018). Currently, our system is limited to acquiring images of seedlings
84 from one side view image but has the advantage of being scalable. Additionally, as this system
85 was developed separately from a greenhouse or growth chamber, it can be used to image
86 concurrently running experiments.

87 Numerous software tools to analyze plant traits from images are available (www.plant-image-
88 analysis.org; Lobet, 2017). The ImageJ plugin HTPheno measures height, width, and area from
89 side-view plant images (Hartmann et al., 2011). Integrated Analysis Platform contains pipelines
90 for multiple plant species and can output measurements such as height, width, skeleton length,
91 volume, convex hull, and number of leaves (Klukas et al., 2014). ImageHarvest measures
92 multiple traits, such as plant dimensions, shoot area, convex hull area, and center of mass
93 (Knecht et al., 2016). PlantCV has functions for multiple shape measurements, such as height,
94 width, perimeter length, center of mass coordinates, and others (Fahlgren et al., 2015; Gehan et
95 al., 2017). The recent addition of a Naive Bayes classifier to PlantCV allows users to quantify
96 color-based features of plants (Gehan et al., 2017). We chose to use PlantCV for plant trait
97 extraction, so that, in addition to morphological features, we could easily quantify leaf necrosis
98 effects of cold stress manifesting as color changes in leaf tissue in our image-based data set.

99   This study sought to compare growth rates of 40 diverse maize inbreds in a mild cold stress
100 treatment under controlled growth conditions using image-based phenotyping methods. We
101 established an image acquisition platform, including a system for embedding metadata and
102 sample tracking, to collect high-quality, standardized RGB images of maize seedlings over time.
103 Trait extraction from images was accomplished using PlantCV. This work describes a robust
104 method for analyzing recovery rates across multiple morphological and color-based traits for a
105 large number of maize inbreds that will serve as a foundation for future work uncovering the
106 genetic basis for cold stress recovery in maize.

107 **Methods**

108 *Plant Material and Growth Conditions*

109 Forty genotypes were used in this study, including: 3IIH6, B73, CM105, CM37, CML052,
110 CML069, CML103, CML228, CML277, D06, DK105, F2, F353, F7, HP301, Il14H, Ki11, Ky21,
111 LH185, LH198, LH82, M162W, M37W, Mo17, Mo18W, MoG, MS71, NC350, NC358, Oh43,
112 Oh7B, P39, PH207, PHJ89, PHP02, Tx303, Tzi8, UH007, W117, and W22. Details for each
113 genotype, such as developer, market class, and population group, are provided in Supplemental
114 Table 1. For all experiments, seeds were planted in 40 cubic inch D-40 DeePots (Stuewe and
115 Sons, Inc.) containing a 1:1 mix of SunGro (Agawam, MA) horticulture professional growing mix
116 and autoclaved field soil approximately 2 inches below the surface. The plants were grown in
117 Conviron growth chambers with a 16 hour 30°C and 8 hour 20°C day/night cycle and watered
118 every other day. The cold stress treatments were implemented using a Thermo Scientific
119 refrigerated incubator programmed with a 16 hour 6°C and 8 hour 2°C day/night cycle. Plants
120 were moved to cold stress conditions approximately 2 hours after dawn at 9 days after sowing
121 (DAS) for the indicated amount of time as required for various experiments. After the indicated
122 time of stress treatment, treated plants were moved from the cold incubator back to growth
123 chambers under control temperature conditions.

124 *Image Acquisition*

125   A Nikon D5100 DSLR Camera with an 18-55mm lens mounted on a Provista 7518B Tripod
126   (Davis & Sanford) produced digital RAW-format images (Figure 1A). A computer running the
127   Ubuntu 14.04 operating system was interfaced with the camera through its universal serial bus.
128   A single shell script that combined gPhoto2 (http://gphoto.org), dcraw
129   https://www.cybercom.net/~dcoffin/dcraw/, tiffcp (http://www.libtiff.org), and MatLab functions
130   controlled image acquisition, assessed image quality, and converted each RAW image file into
131   tagged image file format (TIFF). Custom MatLab code checked that the appropriate camera
132   settings for focal length, f-number, exposure, and body tilt matched defined values. If an image
133   failed the quality and standardization checks, the script identified the problem and prompted the
134   user to retake the image. Approved images in RAW format were automatically stored in a
135   directory corresponding to the date of image acquisition. Sample tracking information and
136   experimental metadata were encoded in a two-dimensional barcode (Quick Response code
137   format) and printed on a piece of paper that was mounted in the scene above the plants (Figure
138   1A). This embedded experimental details and plant identity into the corresponding image data in
139   a machine-readable format. The sample tracking page also contained 24 blue boxes. The user
140   marked the number of blue boxes corresponding to the age of the plants each day they were
141   photographed. This date/age score was automatically added to the sample tracking data at the
142   time of image acquisition.

143   We refer to the three seedlings in each image as a plot. The staging area consisted of a desk, a
144   4'x6' blue drywall background, three plastic D20T racks (Stuewe and Sons, Inc), nails to hold
145   the QR code and day tracking sheets, and the space to the right of the QR code was used to
146   add color standards but could be used for other information as well. The use of DeePots
147   provided several advantages in the system as plants could be grown at high densities and
148   easily moved from growth chambers to the imaging system. Additionally, DeePots enabled
149   plants to be quickly moved in and out of racks, rotated as necessary to adapt to rotations in
150   growth, and placed in consistent locations each day. An example image acquired using this
151   system is depicted in Figure 1B. This system can be used for imaging a wide variety of plant
152   species to obtain side views of plants over time. The combination of imaging platform size and
153   growth conditions allowed for growth and for data to be collected from 8 to 16 days after sowing
154   (DAS). After this time, the growth of the seedlings began to plateau in some genotypes and the
155   leaves of neighboring plants began to overlap, which hindered proper plant segmentation.

156   *Generation of Sample Metadata Tracking Sheets*

157   Custom Perl and R scripts were written to create QR code sheets containing metadata and to
158   allow sample tracking over time. Briefly, a Perl script is run that takes in a tab delimited text file
159   containing the desired sample tracking metadata (plot, genotype, treatment, etc). This Perl
160   script outputs an R script that can be run to produce the formatted QR code sheet with
161   embedded metadata and day tracking boxes. These scripts are available at
162   https://github.com/maizeumn/cold-phenotyping.

163   *Trait extraction from images using PlantCV*

164   Raw .nef format RGB files of maize seedlings were converted to .tiff format files using dcraw
165   (https://www.cybercom.net/~dcoffin/dcraw/). Trait measurements were extracted from each .tiff
166   file using PlantCV v3.0.dev2 (Fahlgren et al., 2015; Gehan et al., 2017;
167   doi:10.5281/zenodo.1408271). Pixel classification within each image was achieved through the
168   use of the Naive Bayes multiclass training module within PlantCV. This approach allowed for
169   color-based classification of plant tissue into two categories: healthy and necrotic, and therefore
170   quantification of the percent area (number of pixels) corresponding to each of these categories
171   (Figure 2A). Plant masks were dilated and filled to reduce noise in the segmentation. Initial
172   efforts to classify plant pixels in this manner resulted in soil pixels being included in the plant

173   necrotic category. Ranges of RGB values for necrotic tissue, stem tissue, and soil overlapped
174   and could not be separated using our training set and the Naive Bayes approach. To remove
175   soil pixels from the plant mask, we identified the rack that held each pot using edge detection
176   methods and excluded any pixels below a boundary line to isolate only plant pixels for later trait
177   extraction. The final plant mask and original RGB image were used to measure attributes of the
178   plant object.

179   Our pipeline used PlantCV to measure 16 morphological traits associated with defined objects,
180   such as height, width, area, convex-hull properties, and various measurements of an object-
181   bounding ellipse (Figure 2B). Height represented the number of pixels from the base of the stem
182   to the tallest point of the plant object. Width captured the number of pixels along a horizontal
183   line between the plant pixel with the smallest x-coordinate to the highest x-coordinate. Area was
184   defined as the number of pixels classified as plant tissue, including pixels in both healthy and
185   necrotic categories. Perimeter represented the number of pixels along the outermost edge of
186   the plant object. Measurements derived from the convex hull included the area of the convex
187   hull, the number of vertices of the convex hull, the longest axis within the convex hull, and
188   solidity. Ellipse-derived measurements included x and y coordinates of the ellipse center, major
189   and minor axis of the ellipse, the rotational angle, and the eccentricity. Traits that were
190   measured by hand had high correlations to the image-derived measurements, suggesting that
191   our image acquisition and trait extraction techniques yielded accurate quantification of these
192   aspects of plant growth. Some morphological traits corresponded to readily explained
193   descriptors of plant morphology, and we chose to focus on traits that were reproducible and
194   captured unique aspects of responses to cold stress in our genotypes. Numerical
195   measurements in pixels for tissue classification categories and morphological traits were written
196   to a .csv file for each image. We chose to output four images for each plant analyzed, which
197   captured various processing steps and documented the quality of plant segmentation
198   (Supplemental Figure 1). The individual .csv output files were merged using a python script, and
199   the data was analyzed in R. Input TIFF format images are available on Cyverse Data Commons
200   (https://doi.org/10.7946/P2T63C). Numerical outputs from PlantCV pipeline as merged .csv files
201   and scripts including R code used to generate figures, Perl code to generate QR code and
202   metadata sheets, and scripts for image acquisition are available here:
203   https://github.com/maizeumn/cold-phenotyping. README files, both on Cyverse for image data
204   and Github for scripts, provide short explanations and usage for each file provided.

205   *Data analysis*

206   <u>Plant Growth Rates</u>

207   For experiments examining the effect of cold stresses of different durations on plant growth,
208   points on line plots represented the mean of six plants per genotype per treatment, and error
209   bars represent standard error of the mean. All experiments were replicated three times with
210   similar results.

211   For experiments surveying responses of genotypes under a 2 day cold stress period, line plots
212   represented the means of n≥14 plants per genotype per treatment at each timepoint. Sample
213   sizes for each genotype for each treatment on each day are indicated in Supplemental Table 2.
214   Where indicated, significance between treatment groups within a genotype was determined by a
215   one-way ANOVA and post-hoc TukeyHSD test to obtain adjusted p-values.

216   <u>Rate calculations</u>

217   The growth rate for indicated time intervals for each unique combination of genotype, treatment,
218   and trait was calculated by finding the slope of a linear regression line for each plant. The slope

219 values were averaged to obtain a single value for each genotype, treatment, trait, and interval
220 group.

Trait clustering

222 The pheatmap function from the R package 'pheatmap' was used to create the heatmap
223 displaying hierarchical clustering of genotypes for each trait for each interval.

Results

Cold stress assay development

226 Cold temperatures often result in slower growth and induce leaf necrosis in maize seedlings, but
227 the severity of these effects varies among genetic backgrounds (Greaves, 1996). The goal of
228 this study was to survey the range of cold stress effects on the growth, morphology, and leaf
229 necrosis across various maize genotypes. The first step towards accomplishing this goal was
230 the design of a cold-stress assay that resulted in phenotypic changes across genetic
231 backgrounds, which also allowed for analysis of recovery within the constraints of our image
232 acquisition system.

233 Our system provided an opportunity to measure plant growth and morphology for maize
234 seedlings from 8 to 16 DAS. We conducted several experiments to identify a set of conditions
235 that allowed analysis of variability for responses to cold stress. A variety of temperatures and
236 stress lengths were assessed to determine appropriate cold stress conditions. While
237 temperatures near or below 0°C provided strong stress responses, we found greater
238 experiment-to-experiment variation and some genotype lethality at these temperatures.
239 Therefore, we elected to use a more moderate low temperature condition (6°C day / 2°C night)
240 that was more phenotypically consistent but resulted in more subtle phenotypes than freezing
241 temperatures. We tested the effects of different durations of this cold stress to select a
242 treatment regime that resulted in observable effects on measured traits but also allowed for
243 quantification of stress recovery in the B73 and Mo17 inbreds (Figure 3). All cold-treated plants
244 were placed in the stress condition two hours after dawn at 9 DAS. Every 24 hours a subset of
245 plants were removed from the cold stress and returned to control conditions in growth chambers
246 for a total of four separate durations of cold treatment ranging from 1 to 4 days. Plants grown
247 under a single 24-hour period of cold treatment had the least amount of growth inhibition in
248 height, area, and width compared to plants grown under control conditions for both genotypes
249 (Figure 3). Four days of cold stress resulted in the most extreme differences in growth
250 compared to control plants for area, height, and width measurements but only allowed for 3 time
251 points during the recovery period. A 2- or 3-day duration of cold stress had intermediate effects
252 to these two extremes. To collect a maximum amount of time points during recovery, a 2-day
253 cold treatment was chosen for further experiments. Additionally, the selection of a 2-day long
254 cold stress over a 1-day cold stress allowed for the analysis of whether any of our selected
255 genotypes were able to grow during the cold period or if the cold stress conditions resulted in
256 growth arrest for all tested genotypes and the collection of five time points to characterize
257 recovery from stress conditions.

Surveying diversity of cold responses using image-based methods

259 To survey the variation in responses to cold stress among diverse genotypes of maize, we
260 implemented a robust cold stress assay that subjected plants to two days of cold stress in
261 growth chamber conditions to analyze cold stress responses in a panel of 40 maize genotypes.
262 Within our selected genotypes, there were representatives from multiple heterotic groups and
263 genotypes that resulted from breeding programs at very distinct latitudes that likely faced
264 variable levels of early season cold stress (Figure 4A; Supplemental Table 1). The genotypes
265 used in this study included 21 of the 25 nested association mapping population parent lines

266 (McMullen et al., 2009), and lines with sequenced genomes such as B73 (Schnable et al., 2009;
267 Jiao et al., 2017), PH207 (Hirsch et al., 2016), W22 (Springer et al., 2018), F7 (Unterseer et al.,
268 2017), and Mo17 (Sun et al., 2018). All plants were grown in conditions described in the
269 methods with a 2-day cold stress as the treatment group. This 2-day cold treatment was able to
270 recapitulate phenotypes observed in field grown plants that experience cold stress, such as leaf
271 necrosis, chlorosis, and growth inhibition. Additionally, our image-based data collection method
272 enabled the capture of nine time points during the early developmental stages of maize plants
273 (Figure 4C, D). Images of Mo17 seedlings grown under control conditions (Figure 4C) and cold-
274 treatment conditions (Figure 4D) provide examples of the developmental time points captured
275 for each seedling and the degree of growth inhibition achieved in our assay. We collected data
276 on three biological replicates that represented different grow-outs. For each biological replicate,
277 we measured traits for six individuals exposed to control conditions and six individuals exposed
278 to a cold stress. In total, this dataset contained images for nine consecutive days of growth for
279 ~18 plants per genotype per treatment resulting in ~12,000 images of ~1,400 plants.

280 Impact of cold stress on leaf necrosis across genotypes

281 One of the more noticeable effects of cold stress in maize seedlings is the appearance of leaf
282 necrosis (Figure 5). Cold temperatures can cause leaf tissue to wilt, and over the course of
283 several days this wilted tissue can die, resulting in changes in leaf color from green to brown
284 and texture from healthy leaves with high turgor to dehydrated, dead leaf tissue (Guye et al.,
285 1987). The Naive Bayes color-based classification module that was trained and implemented
286 within PlantCV classified each plant pixel into a healthy or necrotic category that enabled the
287 quantification of necrosis as a percentage of area belonging to each category for every plant at
288 each time point. The pipeline output included images of each seedling indicating the category
289 each pixel was classified into by color (Figure 2A).

290 Among the genotypes surveyed, we observed substantial variation for this response (Figure 5A,
291 Supplemental Figure 2). Some genotypes, such as Oh43 and NC350, did not exhibit any
292 changes in the proportion of necrotic tissue following a cold stress (Figure 5A). For other
293 genotypes, such as MoG or Ki11, a significant portion of the plant exhibited necrosis. A
294 comparison among these genotypes also revealed variability in the level of necrotic tissue
295 present within the control plants. This resulted from healthy portions of the lower stem having
296 color values with a high probability of being classified as necrosis. This occurred at different
297 frequencies among genotypes. To control for this, we focused on comparing the amount of
298 necrotic tissue in control plants compared to cold stressed plants within each genotype. We also
299 noted variability in the total percent of necrotic tissue during our time series. The percent
300 necrotic value often peaked at 13 DAS followed by a gradual decline. This was a result of new
301 growth of healthy/green tissue following the cold stress, resulting in the overall percent necrotic
302 area decreasing. The percentage of plant area that exhibited necrosis was finite and underwent
303 a predictable sequence of color changes. Therefore, a time-course analysis is unnecessary for
304 this phenotype within our experiments.

305 Accordingly, the percent necrotic tissue was assessed for all 40 genotypes at 13 DAS (Figure
306 5B). Seven genotypes had a significant increase in tissue classified as necrosis relative to the
307 controls. For many of the other genotypes, the cold treatment group never accumulated an
308 amount of necrotic tissue greater than the amount of tissue misclassified as necrotic within the
309 control group. It is worth noting that all genotypes survived the cold stress and continued
310 growth. Even the most severe necrosis responses only resulted in the loss of healthy tissue for
311 two or three leaves.

312 Impact of cold stress on plant morphology across genotypes

313 Genotypes were compared on a single day for quantification of necrotic tissue, however the
314 morphological traits changed at different rates among genotypes, and therefore the entire time
315 course of data collected was utilized (Supplemental Figures 3-7). For example, plant area did
316 not increase during the cold treatment for any genotype (Supplemental Figure 3). Yet, the rate
317 at which area increased following the cold stress period was faster for some genotypes
318 compared to others (Figure 6A, Supplemental Figure 3). Growth rates across traits are more
319 similar within genotypes than among genotypes. The set of traits that are most affected by
320 stress vary across genotypes. Values for all analyzed morphological traits did not appear to
321 increase during the cold treatment for any genotype but recovery rates following the stress
322 varied. Because genotypes are not growing during the cold stress period, they are delayed in
323 development compared to plants grown under control conditions. Because of the cold-induced
324 delay in growth, a more equivalent comparison than comparing control and cold-stressed data
325 at the same time point was to compare cold-stressed data to control data at a time point two
326 days earlier. Therefore, we chose to compare measurements for morphological traits with a
327 time-shifted approach, comparing the cold-stress plant measurements to the control plant
328 measurements collected 2 days prior for each genotype (Figure 6B). This allowed comparisons
329 of control and cold stressed plants at more similar developmental stages. Additionally, to
330 minimize the effects of individual plant size on comparisons, we calculated growth rates during
331 two intervals among the time-shifted data (Figure 6C). Within each interval, we calculated the
332 $\log_2$ fold change in growth rates between treatments for each genotype for each trait.

333 Clustering genotypes based on leaf necrosis and morphology phenotypes

334 Because of intrinsic morphological differences among genotypes, growth rates manifest in
335 different patterns across traits. Therefore, a phenotype fingerprint, or phingerprint, captures the
336 unique aspects of cold response in each genotype. The time-shifted and normalized data from
337 plant morphology phenotypes and the percent necrosis data from day 13 was used to cluster
338 genotypes using hierarchical clustering (Figure 7). This resulted in three clusters. Overall
339 patterns of growth inhibition were fairly similar across all genotypes. However, subtle differences
340 among degrees of fold change and the pattern of changes across different morphological traits
341 helped define genotypes into different clusters. One cluster was characterized by more subtle
342 changes in growth rates compared to controls of morphological traits over the two defined
343 intervals. A second cluster was dominated by higher degrees of necrosis than controls on day
344 13. A third cluster was characterized by moderate levels of necrosis on day 13 and a smaller
345 fold change in growth rate of height compared to controls. Our initial hypothesis was that
346 genotypes may cluster together based on some attributes, such as population group, market
347 class, kernel type, or latitude. This did not appear to be the case. Latitude did not have a
348 significant correlation with any of the $\log_2$ fold changes in growth rates for any traits during either
349 interval. Therefore, cold sensitivity during early development was likely not a target of breeding
350 programs for these genotypes.

Discussion

352 Improving cold tolerance in maize remains a challenge, despite nearly 100 years of studies.
353 Phenotyping approaches can enable new insights into cold stress responses in plants. This
354 study successfully used image-based phenotyping methods to characterize how maize
355 seedlings respond and recover from a cold stress event. Our approach allowed comparisons of
356 multiple genotypes over time and for quantitative measurements of cold stress responses, such
357 as area, height, width, and development of leaf necrosis. The quantification of these traits from
358 images facilitated nondestructive measurements to be made over time and enabled our analysis
359 of recovery rates. The use of hierarchical clustering allowed for a methodical approach to
360 compare the ability of genotypes to recover from cold stress.

361 As with most image-based time course phenotyping methods, there were several limitations to
362 our approach. The patterns of clustering were influenced by the choice of time intervals and
363 included traits. Every inbred in our study is sensitive to cold, so differences among that
364 sensitivity can be subtle. The quantification of the leaf necrosis phenotype provided a
365 straightforward definition of the most cold sensitive genotypes within our assay, however the
366 morphological traits captured subtle variations in the diverse patterns of cold response.
367 Additionally, although our assay recapitulates phenotypes observed in field-grown plants that
368 experience cold stress (chlorotic bands on leaves and leaf necrosis), caution must be made
369 when extrapolating controlled-condition studies to field conditions. Finally, the performance of
370 inbreds does not always predict combining ability for hybrids, so future studies could include
371 analysis of heterosis among various hybrids for recovery from cold stress.

372 Many studies suggested flint genotypes are more cold tolerant than dent genotypes across a
373 number of different cold assays and developmental stages (Bhosale et al., 2007; Riva-Roveda
374 et al., 2016). With our approach, flint and dent genotypes did not classify into separate clusters,
375 although dent genotypes did appear to have more severe necrosis than flint genotypes. Ki11, a
376 flint genotype, exhibits the highest percentage of necrosis of all genotypes in our study. Other
377 examples violating the assumption that dent genotypes are cold sensitive exist, such as a
378 favorable allele for cold tolerance being identified in a European dent line (Strigens et al., 2013).
379 Additionally, in a large study comparing cold tolerance of flint and dent varieties of European
380 origin, genotypes with a high degree of cold tolerance were found among both dent and flint
381 groups (Revilla et al., 2014). The same study found no strong pattern among cold tolerance and
382 latitude of geographical origin, which is also consistent with our results.

383 Assigning a latitude and other attributes, such as kernel texture and population group, to maize
384 inbreds can be a difficult task. Many genotypes have complex pedigrees, making distinct
385 category assignments inaccurate or not representative of breeding history. For example, Mo17
386 was developed in the state of Missouri in the United States; however, lines used to generate
387 Mo17 were developed in both Illinois and Connecticut (Andorf et al., 2016). This example
388 illustrates how assigned geographical regions of maize inbreds may not be straightforward and
389 could help explain the lack of correlation between our measures of cold sensitivity and latitude.
390 Alternatively, it is possible that different breeders utilized different practices in terms of planting
391 date. Breeders that preferred to plant earlier in the season likely imposed some selection for
392 early season cold tolerance while breeders that planted later in the season likely did not impose
393 this selective pressure.

394 Few studies have analyzed responses to cold stress in maize over time. One recent study that
395 performed time-series analysis of leaf elongation rates under a cold stress used manual
396 methods to collect this data (Riva-Roveda et al., 2016). Measurements collected using image-
397 based phenotyping can greatly reduce the amount of time and labor needed to investigate how
398 traits change over time, as well as archive plant morphology for future studies. Our approach
399 enabled the simultaneous collection of multiple morphological and color-based measurements
400 at nine time points for thousands of individual plants. Having daily imaging and quick trait
401 extraction pipelines allowed us to collect a large amount of phenotypic data on many plants.
402 Using these techniques, we recognized the delay in growth rates the stress caused, and
403 therefore we compared treatment groups at more equivalent developmental stages. This
404 analysis would not have been possible if we had made measurements at fewer time points.

405 Our goal was to provide a basis for designing genetic mapping studies to work towards
406 maximizing the ability of maize to withstand and recover from early season cold stress events.
407 Additional future studies could include a cold acclimation period and analyzing whether this
408 impacts recovery rates, leaf necrosis, and the clustering of genotypes. Image-based
409 phenotyping methods can provide more in-depth analysis of cold stress responses in maize and

410   may help tease apart the narrow genetic variance for cold tolerance in this important crop
411   species.

References

413   **Aguilera C, Stirling CM, Long SP** (1999) Genotypic variation within Zea mays for susceptibility
414   to and rate of recovery from chill-induced photoinhibition of photosynthesis. Physiol Plant
415   **106**: 429–436

416   **Andorf CM, Cannon EK, Portwood JL 2nd, Gardiner JM, Harper LC, Schaeffer ML, Braun
417   BL, Campbell DA, Vinnakota AG, Sribalusu VV, et al** (2016) MaizeGDB update: new
418   tools, data and interface for the maize model organism database. Nucleic Acids Res **44**:
419   D1195–201

420   **Armoniené R, Odilbekov F, Vivekanand V, Chawade A** (2018) Affordable Imaging Lab for
421   Noninvasive Analysis of Biomass and Early Vigour in Cereal Crops. Biomed Res Int **2018**:
422   5713158

423   **Bhosale SU, Rymen B, Beemster GTS, Melchinger AE, Reif JC** (2007) Chilling tolerance of
424   Central European maize lines and their factorial crosses. Ann Bot **100**: 1315–1321

425   **Capell B, Dörffling K** (1993) Genotype-specific differences in chilling tolerance of maize in
426   relation to chilling-induced changes in water status and abscisic acid accumulation. Physiol
427   Plant **88**: 638–646

428   **Czedik-Eysenberg A, Seitner S, Güldener U, Koemeda S, Jez J, Colombini M, Djamei A**
429   (2018) The "PhenoBox", a flexible, automated, open-source plant phenotyping solution.
430   New Phytol **219**: 808–823

431   **Fahlgren N, Feldman M, Gehan MA, Wilson MS, Shyu C, Bryant DW, Hill ST, McEntee CJ,
432   Warnasooriya SN, Kumar I, et al** (2015) A Versatile Phenotyping System and Analytics
433   Platform Reveals Diverse Temporal Responses to Water Availability in Setaria. Mol Plant **8**:
434   1520–1535

435   **Fracheboud Y, Haldimann P, Leipner J, Stamp P** (1999) Chlorophyll fluorescence as a
436   selection tool for cold tolerance of photosynthesis in maize (Zea mays L.). J Exp Bot **50**:
437   1533–1540

438   **Gehan MA, Fahlgren N, Abbasi A, Berry JC, Callen ST, Chavez L, Doust AN, Feldman MJ,
439   Gilbert KB, Hodge JG, et al** (2017) PlantCV v2: Image analysis software for high-
440   throughput plant phenotyping. PeerJ **5**: e4088

441   **Greaves JA** (1996) Improving suboptimal temperature tolerance in maize- the search for
442   variation. J Exp Bot **47**: 307–323

443   **Guye MG, Vigh L, Wilson JM** (1987) Recovery after Chilling: An Assessment of Chill-
444   Tolerance in Phaseolus spp. J Exp Bot **38**: 691–701

445   **Hartmann A, Czauderna T, Hoffmann R, Stein N, Schreiber F** (2011) HTPheno: an image
446   analysis pipeline for high-throughput plant phenotyping. BMC Bioinformatics **12**: 148

447   **Hetherington SE, Oquist G** (1988) Monitoring chilling injury: A comparison of chlorophyll
448   fluorescence measurements, post-chilling growth and visible symptoms of injury in Zea

449 mays. Physiol Plant **72**: 241–247

450 **Hirsch CN, Hirsch CD, Brohammer AB, Bowman MJ, Soifer I, Barad O, Shem-Tov D,**
451 **Baruch K, Lu F, Hernandez AG, et al** (2016) Draft Assembly of Elite Inbred Line PH207
452 Provides Insights into Genomic and Transcriptome Diversity in Maize. Plant Cell **28**: 2700–
453 2714

454 **Janowiak F, Dörffling K** (1996) Chilling of Maize Seedlings: Changes in Water Status and
455 Abscisic Acid Content in Ten Genotypes Differing in Chilling Tolerance. J Plant Physiol **147**:
456 582–588

457 **Janowiak F, Luck E, Dörffling K** (2003) Chilling Tolerance of Maize Seedlings in the Field
458 during Cold Periods in Spring is Related to Chilling-Induced Increase in Abscisic Acid
459 Level. Journal of Agronomy and Crop Science **189**: 156–161

460 **Jiao Y, Peluso P, Shi J, Liang T, Stitzer MC, Wang B, Campbell MS, Stein JC, Wei X, Chin**
461 **C-S, et al** (2017) Improved maize reference genome with single-molecule technologies.
462 Nature **546**: 524–527

463 **Klukas C, Chen D, Pape J-M** (2014) Integrated Analysis Platform: An Open-Source Information
464 System for High-Throughput Plant Phenotyping. Plant Physiol **165**: 506–518

465 **Knecht AC, Campbell MT, Caprez A, Swanson DR, Walia H** (2016) Image Harvest: an open-
466 source platform for high-throughput plant image processing and analysis. J Exp Bot **67**:
467 3587–3599

468 **Kucharik CJ** (2008) Contribution of Planting Date Trends to Increased Maize Yields in the
469 Central United States. Agron J **100**: 328–336

470 **Lobet G** (2017) Image Analysis in Plant Sciences: Publish Then Perish. Trends Plant Sci **22**:
471 559–566

472 **Lyons JM** (1973) Chilling Injury in Plants. Annu Rev Plant Physiol **24**: 445–466

473 **Marocco A, Lorenzoni C, Francheboud Y** (2005) Chilling stress in maize. Maydica **50**: 571

474 **McMullen MD, Kresovich S, Villeda HS, Bradbury P, Li H, Sun Q, Flint-Garcia S,**
475 **Thornsberry J, Acharya C, Bottoms C, et al** (2009) Genetic properties of the maize
476 nested association mapping population. Science **325**: 737–740

477 **Miedema P** (1982) The Effects of Low Temperature on Zea mays. *In* NC Brady, ed, Advances
478 in Agronomy. Academic Press, pp 93–128

479 **Revilla P, Rodríguez VM, Ordás A, Rincent R, Charcosset A, Giauffret C, Melchinger AE,**
480 **Schön C-C, Bauer E, Altmann T, et al** (2014) Cold Tolerance in Two Large Maize Inbred
481 Panels Adapted to European Climates. Crop Sci **54**: 1981

482 **Riva-Roveda L, Escale B, Giauffret C, Périlleux C** (2016) Maize plants can enter a standby
483 mode to cope with chilling stress. BMC Plant Biol **16**: 212

484 **Sánchez B, Rasmussen A, Porter JR** (2014) Temperatures and the growth and development
485 of maize and rice: a review. Glob Chang Biol **20**: 408–417

486 **Schnable PS, Ware D, Fulton RS, Stein JC, Wei F, Pasternak S, Liang C, Zhang J, Fulton**
487   **L, Graves TA, et al** (2009) The B73 maize genome: complexity, diversity, and dynamics.
488   Science **326**: 1112–1115

489 **Sellschop JPF, Salmon SC** (1928) The Influence of Chilling, Above the Freezing Point, on
490   Certain Crop Plants. Journal of Agricultural Research **37**: 315–388

491 **Sowiński P, Rudzińska-Langwald A, Adamczyk J, Kubica I, Fronk J** (2005) Recovery of
492   maize seedling growth, development and photosynthetic efficiency after initial growth at low
493   temperature. J Plant Physiol **162**: 67–80

494 **Springer NM, Anderson SN, Andorf CM, Ahern KR, Bai F, Barad O, Barbazuk WB, Bass**
495   **HW, Baruch K, Ben-Zvi G, et al** (2018) The maize W22 genome provides a foundation for
496   functional genomics and transposon biology. Nat Genet **50**: 1282–1288

497 **Strigens A, Freitag NM, Gilbert X, Grieder C, Riedelsheimer C, Schrag TA, Messmer R,**
498   **Melchinger AE** (2013) Association mapping for chilling tolerance in elite flint and dent
499   maize inbred lines evaluated in growth chamber and field experiments. Plant Cell Environ
500   **36**: 1871–1887

501 **Sun S, Zhou Y, Chen J, Shi J, Zhao H, Zhao H, Song W, Zhang M, Cui Y, Dong X, et al**
502   (2018) Extensive intraspecific gene order and gene structural variations between Mo17 and
503   other maize genomes. Nat Genet **50**: 1289–1295

504 **Tisné S, Serrand Y, Bach L, Gilbault E, Ben Ameur R, Balasse H, Voisin R, Bouchez D,**
505   **Durand-Tardif M, Guerche P, et al** (2013) Phenoscope: an automated large-scale
506   phenotyping platform offering high spatial homogeneity. Plant J **74**: 534–544

507 **Unterseer S, Seidel MA, Bauer E, Haberer G, Hochholdinger F, Opitz N, Marcon C, Baruch**
508   **K, Spannagl M, Mayer KFX, et al** (2017) European Flint reference sequences complement
509   the maize pan-genome. bioRxiv 103747

510 **Verheul MJ, Picatto C, Stamp P** (1996) Growth and development of maize (Zea mays L.)
511   seedlings under chilling conditions in the field. Eur J Agron **5**: 31–43

512 **Wijewardana C, Hock M, Henry B, Reddy KR** (2015) Screening Corn Hybrids for Cold
513   Tolerance using Morphological Traits for Early-Season Seeding. Crop Sci **55**: 851–867

514 **Yadav SK** (2010) Cold stress tolerance mechanisms in plants. A review. Agron Sustain Dev **30**:
515   515–527

516 ## Acknowledgments

520 ## Author Contributions

521 N.M.S., C.D.H., and T.A.E. designed the research; T.A.E., S.S.D., and J.O. performed research;
522 S.T.C., N.D.M., C.D.H. contributed new computational tools; T.A.E. analyzed data; T.A.E.,
523 N.M.S., and C.D.H. wrote the paper. All authors commented on and approved the final
524 manuscript.

Figure Legends

Figure 1. Schematic of the RGB imaging system. A) The imaging system consisted of a DSLR camera, computer, back lighting, blue background, and three racks to hold pots. Metadata for each image was stored in a QR code and day after sowing was crossed off on a sheet of paper hung on the top left of the background in each image. A color standard was also included for use in image analysis pipelines. B) Representative example of an acquired image.

Figure 2. Extracted traits. A) False-colored image indicating the quantification of the areas classified as necrotic (brown) and healthy (green) tissue. B) Plant with overlaid representative measured morphological traits.

Figure 3. Mean growth rates of traits for B73 and Mo17 control and cold-stressed seedlings. Cold stressed seedlings were transferred to a separate incubator with a 6°C/2°C day/night cycle on day 9 after sowing, and stressed for the indicated amount of time (1, 2, 3, or 4 days), then returned to the control-temperature growth chamber. Error bars represent standard error of the mean of 6 plants.

Figure 4. Experimental design to survey genotypic responses to cold stress. A) Latitudes of source location of the 40 inbred genotypes included in this study. B) Plants were grown under a 30°C 16-hour day and 20°C 8-hour night cycle. At 9 days after sowing, cold-stressed plants were placed in a low-temperature incubator under a 6°C 16-hour day and a 2°C 8-hour night until 11 days after sowing and returned to the control conditions. RGB images of the plants were collected between 9:00 am and 12:00 pm each day. C) Image masks of a Mo17 control plant at each time point. D) Image masks of Mo17 cold-stressed plant at each time point.

Figure 5. Percent necrosis over time. A) Mean percent necrosis for each time point for 6 maize genotypes. Error bars represent standard error of the mean. B) Mean percent necrosis on day 13 for 40 maize genotypes. Error bars represent standard error of the mean. Data shaded with a gray box had an adjusted p-value of ≤ 0.05 in a one-way ANOVA and post-hoc Tukey test.

Figure 6. Morphological traits over time and calculations for clustering. A) Mean area for each time point for 7 maize genotypes used in this study. B) Data presented in panel A with 2 days shift back in time for cold-treated samples. C) Selection of time intervals for comparing growth rates during equivalent developmental stages of control and cold-treated plants.

Figure 7. Phingerprints classify maize inbreds into three clusters. Each cell represents the $\log_2$ fold change in growth rate between control and cold-treated plants for the trait and interval indicated for each row.

Supplemental Data

Supplemental Table 1. Information about each genotype.

Supplemental Table 2. Sample size information.

Supplemental Figure 1. Image output from PlantCV pipeline. A) Merged image indicates pixels categorized as healthy (blue) or necrotic (red). B) Final plant binary mask used for shape and color analysis. C) Output from PlantCV analyze_object function. D) Output from PlantCV analyze_color function false colored using the "value" channel from HSV colorspace.

Supplemental Figure 2. Mean values for percent necrosis at each time point for 40 maize inbred genotypes. Error bars represent standard error of the mean.

Supplemental Figure 3. Mean values for plant area at each time point for 40 maize inbred genotypes. Error bars represent standard error of the mean.
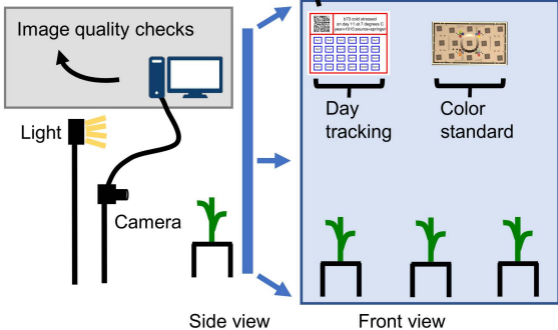
568   Supplemental Figure 4. Mean values for plant height at each time point for 40 maize inbred
569   genotypes. Error bars represent standard error of the mean.

570   Supplemental Figure 5. Mean values for plant width at each time point for 40 maize inbred
571   genotypes. Error bars represent standard error of the mean.

572   Supplemental Figure 6. Mean values for plant perimeter at each time point for 40 maize inbred
573   genotypes. Error bars represent standard error of the mean.

574   Supplemental Figure 7. Mean values for plant hull area at each time point for 40 maize inbred
575   genotypes. Error bars represent standard error of the mean.

A

Image quality checks

QR code: sample tracking

Light

Camera

Day tracking

Color standard

Side view

Front view

B

Legend: Control, 1 d, 2 d, 3 d, 4 d

A

B

C

D

A

B

C

1. early recovery:

$$\log_2\left(\frac{m_{\text{Cold days 11-13}}}{m_{\text{Control days 9-11}}}\right)$$

2. late recovery:

$$\log_2\left(\frac{m_{\text{Cold days 13-16}}}{m_{\text{Control days 11-14}}}\right)$$